

Direct Conversion of N-Acetyl-D-glucosamine to N-containing heterocyclic compounds 3-acetamidofuran and 3-acetamido-5-acetyl furan.

Samrin Shaikh

CSIR-National Chemical Laboratory: National Chemical Laboratory CSIR

Chetana Patil

CSIR-National Chemical Laboratory: National Chemical Laboratory CSIR

Nishita Lucas

CSIR-National Chemical Laboratory: National Chemical Laboratory CSIR

Vivek Bokade

CSIR-National Chemical Laboratory: National Chemical Laboratory CSIR

Chandrashekar Rode (✉ cv.rode@ncl.res.in)



CSIR-NCL: National Chemical Laboratory CSIR <https://orcid.org/0000-0002-2093-2708>

Research Article

Keywords: Lanthanum oxide, N-Acetyl-D-glucosamine, heterogeneous catalysis, dehydration, renewable feedstock, 3-acetamidofuran, 3-acetamido-5-acetylfuran

Posted Date: November 28th, 2022

DOI: <https://doi.org/10.21203/rs.3.rs-2246084/v1>

License:   This work is licensed under a Creative Commons Attribution 4.0 International License. [Read Full License](#)

Version of Record: A version of this preprint was published at Waste and Biomass Valorization on April 11th, 2023. See the published version at <https://doi.org/10.1007/s12649-023-02127-2>.

Abstract

Effectual waste utilization from plant as well as marine biomass has gained tremendous importance with reference to sustainability. The valorization of marine biomass produces value added compounds containing not only C, H, O but also renewable N atom in the skeleton which widens the scope for its exploration which may prove to be economically beneficial to the society. Heterogeneous catalytic transformation of marine biomass i.e. N-acetyl glucosamine (NAG) to N-substituted aromatic heterocyclic is reported for the very first time. Cost effective and stable metal oxide catalysts were deployed for the transformation. Catalyst screening study showed that La_2O_3 was found to be an excellent catalyst for N-acetyl glucosamine (NAG) dehydration which mainly produced 3-acetamidofuran (3AF). The physicochemical properties of the metal oxide catalyst were investigated by various techniques such as XRD, FTIR, MeOH-FTIR, TPD, SEM, N_2 sorption studies and HR-TEM analysis for structure activity relationship. The effect of various reaction parameters such as catalyst concentration, reaction temperature, reaction time and solvent effect on dehydration of N-acetyl glucosamine has been studied in detail for higher yields. The results revealed that the presence of weak basic sites which are Brønsted in nature and nano pores present on the surface were responsible for improved dehydration of the chitin biomass to selectively yield 3-acetamidofuran (3AF). La_2O_3 catalyst showed optimum 50% 3AF yield from N-Acetyl glucosamine at 180 °C in 3h. Efficacious exploitation of marine biomass to value added chemicals using heterogeneous catalyst through simple route and easy separation of N-substituted heterocyclic aromatics is the most innovative aspect of the current study. Thus, utilization of heterogeneous catalyst and renewable biomass as a raw material indicates a transition towards more sustainable and greener approach.

Statement Of Novelty

As marine biomass is abundantly available on valorization widens its scope for production of value added products and platform chemicals. As far as sustainability and green synthesis is concerned we report for the first time dehydration of NAG to renewable N-containing furan derivatives by heterogeneous catalyst without use of any additives, ionic liquids or boron compounds. The catalyst showed high stability, easy separation and excellent recyclability upto 5 cycles. The co-operative effect of Brønsted basicity and nanopores on the catalyst play vital role in (100 %) NAG conversion to yield 50 % 3AF and 20 % 3A5AF. 3AF and 3A5AF may find application as precursors for the synthesis of naturally occurring antibiotic and antitumor drug proximycin A, B and C, amino sugars, pyridine derivatives etc.

Introduction

Efficient waste valorization has been in limelight as it could aid the society to mitigate the alarming environmental issues arising due to the depletion of fossil fuels such as energy crises, green house effects etc.⁽¹⁻³⁾ Among the biomass variants, marine biomass is readily available as oceans occupy around 71% of earth's surface. But for decades, the advancement and valorization of marine biomass has remained unexplored, which could emerge as a strong feedstock to bring sustainability and economic benefit to the society. After cellulosic biomass, chitin stands second most abundant biomass on earth with 100 billion tons produced annually.⁽⁴⁾ Chitin biomass is obtained from shells of several marine animals like crabs, lobsters, shrimps, crayfish, arthropods as well as from cell wall of fungi and yeast.⁽⁵⁻⁷⁾ Cellulosic biomass on valorization produces value added compounds containing mainly C, H, and O. Whereas, the marine biomass on valorization widens the scope for production of N-containing platform chemicals having various applications as adsorbents, waste water treatment, agricultural chemicals, polymers, food industries, biomedical applications, formation of films, fibers, composites and cosmetics.⁽⁸⁻¹⁰⁾ Chitin biomass comprises of N-Acetyl glucosamine units linked through β -1, 4 glycosidic linkages to form polymeric chains in three different

allomorphic forms α , β , γ . Therefore, the chitin biomass exhibits distinct physicochemical properties due to the presence of N-functionality in its skeleton and serves as most important natural source of nitrogen.^(8,11-13) Cellulosic biomass and chitin biomass have structural similarities with the exception that cellulosic biomass on valorization produces value added compounds and platform chemicals containing C, H and O whereas, chitin biomass produces chemicals containing C, H, O and N. Owing to the presence of 7 wt. % renewable N atom in chitin it has put the marine biomass on fame and has attracted the attention of researchers as it has tremendous scope for its valorization with wide range of applications.⁽¹⁴⁻¹⁵⁾ The chitin hydrolysis is carried out by biological, physical and chemical pretreatment methods which produces NAG, which requires number of steps and harsh conditions like use of mineral acids, high temperature and, thus suffers from major drawbacks making process non feasible. Also, the biological methods fail to eliminate the minerals and proteins from the crustacean shells and high cost of enzymes makes the process less cost effective.⁽¹⁶⁻¹⁷⁾ Prior to chitin hydrolysis, microwave irradiation and sonication were used to increase the chitin solubility in HCl thereby enhancing the chitin hydrolysis to produce NAG.⁽¹⁸⁻¹⁹⁾ Franich et al. reported for the first time that the pyrolysis of tar produced several degradation products with 5% 3-acetamidofuran (3AF), 2% 3-acetamido-5-acetyl furan (3A5AF) and 3% 3-acetamidoacetaldehyde yield.⁽²⁰⁾ Chen et al. studied the NAG pyrolysis at 200 °C for 30 min to produce 3A5AF as the major product with 3AF and several furanic and pyrazine derivatives as minor products. The pyrolysis pathway results in the formation of number of products thus making the process less economical due to lower selectivity towards product formation.⁽¹⁶⁾ The platform chemical 3A5AF, is a precursor for the synthesis of an anticancer drug proximycin A.⁽²¹⁻²²⁾ Both the products 3AF and 3A5AF have N-containing amide functionality in the form of furanic aromatic platform chemicals which can further be explored for their transformations to value added products. But the challenge is retention of amide group as it easily gets fragmented from the main chain.⁽²³⁾ 3AF and 3A5AF may find a role as synthetic precursors for the synthesis of naturally occurring antibiotic and antitumor drug proximycin A, B and C and amino sugars, amino acids and dihydrodifuro pyridine derivatives, aminated bicyclic ethers, pyridine derivatives, bicyclic pyrrolidines via various multi step organic transformations due to its structural similarity and presence of N atom in its skeleton.⁽²⁴⁻²⁸⁾ 3A5AF on asymmetric reduction, produced (3-acetamido-5-(1-hydroxyethyl)furan, a precursor for the synthesis of amino sugar L-rednose which is a precursor forming the structural unit of biologically active natural products such as Anthracycline⁽²⁹⁾, Saquamycin⁽³⁰⁾ and Rudolphomycin.⁽³¹⁾ Ha et al. reported chemoenzymatic dehydration of NAG and its further enantioselective asymmetric reduction to 3-Acetamido-5-(1-hydroxyethyl)furan(3A5HEF) with good yield.⁽³²⁾ Omari et al. reported the conversion of NAG to 3A5AF in the presence of B(OH)₃ and NaCl under high temperature microwave irradiation (220 °C for 15 min) to give 58% 3A5AF yield. His group highlighted the importance of the presence of chloride and boron atoms in the hydrolysis of chitin and dehydration of NAG to 3A5AF, respectively.⁽²¹⁾ Drover et al. studied the transformation of NAG into 3A5AF with 60% yield under microwave heating with ionic liquid, [BMIM]Cl in which imidazolium ring was found to play an important role in the conversion of NAG to 3A5AF.⁽³³⁾ Chen et al. introduced the acidic proton at C-2 position and reported the importance of Cl anion in the solubility and dissolution of chitin thereby accelerating its hydrolysis to yield value added products. They reported the direct conversion of chitin to 3A5AF with 7% yield in ionic liquid using boric acid and HCl as an additive.⁽³⁴⁾ Wang et al. reported conversion of chitin to yield 43% 3A5AF in glycine chloride ionic liquid.⁽³⁵⁾ Hence, ionic liquids can be used as ideal solvents as they can bare high temperature range, non-volatile and are non-inflammable. But certain disadvantages like toxicity, handling difficulty and higher cost make ionic liquids less economical for use.⁽³⁶⁾ Surprisingly, the synthesis of furanic compounds remains unexplored using heterogeneous catalysts which excel others in cost, recyclability, ease of separation, catalyst tunability and process improvisation. Visualizing the importance of the marine waste valorization and advantages of the heterogeneously catalyzed conversion, the current study gives first hand report on dehydration and partial deoxygenation of NAG to N-containing renewable platform molecules using various metal oxide catalysts.

Choice of catalyst originated from some striking features like stability, cost effectiveness and ease of preparation. A comparative study of acid and basic catalysts has been attempted to furnish insights into type of sites required for selective formation of furans. The best catalyst was characterized by XRD, FTIR, MeOH-FTIR and SEM along with effect of reaction parameters on NAG dehydration to produce 3AF has been carried out.

Experimental

2.1. Materials

N-acetyl glucosamine, lanthanum oxide (La_2O_3), calcium oxide (CaO), cerium oxide (Ce_2O_3), zirconium oxide (ZrO_2), aluminium oxide (Al_2O_3) and barium hydroxide (BaOH_2) were purchased from Thomas Baker Chemicals, India. The chemicals were used as received without further purification. The solvents such as MeOH, DMF, DMSO, ACN, n-Hexane, EtOAc, DMA, MIBK, dioxane and other chemicals were also purchased from HIMEDIA chemicals, India. DMSO-d₆ was purchased from Sigma Aldrich, India and was used as NMR solvent.

2.2. Catalyst Preparation

Barium hydroxide was calcined at 550 °C for 6 h to produce barium oxide.

2.3. Catalyst Characterization

The catalyst was characterized by using various techniques. The X-ray diffraction (XRD) analysis was carried out on a P Analytical PXRD system (Model X-Pert PRO-1712), using Ni filtered Cu K α radiation ($\lambda = 0.154 \text{ nm}$) as an X-ray source (current intensity, 30 mA; voltage, 40 kV) and an X-accelerator detector. XRD measurements were carried out in a 2θ range of 5°–85° with a scanning rate of 5 °/min. The SEM-EDAX analysis was carried out in order to study the morphology and elemental composition of the catalysts on a LEO – LEICA STEREOSCAN 440 instrument. Prior to the analysis the powdered samples were dispersed in iso-propanol and sonicated for 15 minutes. Then drops of the suspension were deposited on a carbon-coated copper grid and dried, at room temperature. The samples were gold coated before analysis. HR-TEM analysis was carried out on JEOL 1200 EX model which provided information about the morphology, particle size, d-spacing and fringe width. Prior to the analysis the powdered samples were dispersed in iso-propanol and sonicated for 15 minutes. Then drops of the suspension were deposited on a carbon-coated copper grid dried, at room temperature before analysis. FTIR spectra of the catalysts were done on a Perkin Elmer 2000 FTIR spectrometer in the range of 4000 – 400 cm^{-1} . The surface areas of all the catalysts using BET equation were measured on Quantachrome v 2.0 instrument. The basic sites present on the catalyst surface were quantitatively analyzed by CO_2 -TPD carried out on Micromeritics-2720 (ChemisoftTPx) volumetric instrument. The samples were pre-treated from room temperature to 200 °C under a helium flow rate of 25 mL min^{-1} followed by CO_2 adsorption at 40 °C and finally CO_2 desorption with heating rate of 10 °C min^{-1} starting from adsorption temperature to 700 °C. The TGA analysis of the catalyst was carried out on Simultaneous Thermal Analyzer SDT-650 apparatus. The analysis was carried out in air (40 mL min^{-1}) at a heating rate of 10 °C min^{-1} from room temperature to 800 °C.

2.4. Catalyst Activity Measurement

In a 50 mL Parr reactor, N-Acetyl-glucosamine (1 gm), dioxane (25 mL) and catalyst (200 mg) were heated at 180 °C under constant stirring for 4 h. After the reaction was complete, the reaction mixture was filtered and the filtrate was

concentrated on BuchiRotavap at 140 mbar and 60 °C. Yellowish-red viscous liquid was obtained from which product was separated by solvent extraction using ethyl acetate and water. The humins were separated in water layer whereas the product was extracted in the ethyl acetate layer. The crude product thus obtained was then purified by silica gel column chromatography. The detailed procedure for isolation of 3AF and 3A5AF are given in supplementary material. **Fig.sS1a, S1b, S2a and S2b** show ^1H NMR and ^{13}C NMR spectra of the isolated 3A5AF and 3AF, respectively. **Fig.sS3 and S4** represent the HR-MS chromatograms of 3AF and 3A5AF and **Fig.sS5 and S6** shows FTIR (NAG and 3AF, 3A5AF) analysis qualitatively. The NAG conversion was analyzed by HPLC (Agilent 1260) equipped with Hiplax-Pb column (300 mm length) equipped with refractive index detector. Deionized water (DI) was used as a mobile phase, which was filtered and used. The NAG conversion was quantitatively determined by HPLC analysis by keeping 0.5 mL/min flow rate of the prepared mobile phase maintaining column temperature at 80 °C and total analysis time of 20 minutes. The products formed were identified and confirmed by HRMS, ^1H and ^{13}C NMR. The calibration curve is given in supplementary material **Fig.S7**.

Recycling Of Catalyst

At the end of reaction, the catalyst was recovered by filtration and washed four times with 10 mL DI water until pale yellow coloured impurities faded, then dried at 110 °C overnight in a vacuum oven followed by calcination at 550 °C for 3 h and reused. In order to determine the reusability and stability of the catalyst, the recovered catalyst was characterized by XRD, FTIR and TGA.

Results And Discussion

3.1. Catalyst characterization

Figure 1b shows the powder XRD pattern for the metal oxide catalysts. The wide angle XRD patterns of the sample of La_2O_3 showed reflections at $2\theta = 15.70^\circ, 27.18^\circ, 28.09^\circ, 39.41^\circ, 48.2^\circ$ ascribed to La_2O_3 phase [JCPDS # 05-0602] corresponding to (100), (002), (101), (102), (211) planes, respectively, with lattice constants as $a = 3.397$ nm and $b = 6.129$ nm which indicated the presence of hexagonal phase of La_2O_3 [JCPDS # 05-0602].⁽³⁷⁾ The diffraction peaks at $2\theta = 15.70^\circ$ and 48.80° can be indexed to the hexagonal phase of $\text{La}(\text{OH})_3$ corresponding to (100) and (211) planes with lattice constants as $a = 0.652$ nm and $b = 0.858$ nm.⁽³⁸⁾ The appearance of sharp peaks for the hexagonal phases of La_2O_3 and LaOH_3 denote high crystallinity of La_2O_3 . La_2O_3 didn't show typical peak for carbonated form of lanthanum which can be observed at $2\theta = 10.2^\circ$, it confirmed the presence of La_2O_3 phase and small amount of $\text{La}(\text{OH})_3$ phase in the examined sample.⁽³⁹⁾ All the other catalysts used for comparison also showed well defined phase. The wide angle XRD pattern for tetragonal phase of BaO showed the reflections at $2\theta = 19.6^\circ, 23.7^\circ, 45.1^\circ$, [JCPDS#47-1488]. Whereas, reflections at $2\theta = 23.7^\circ, 29.1^\circ$ and 55.8° were ascribed to monoclinic ZrO_2 phase [JCPDS#86-1451].⁽⁴⁰⁾ The XRD pattern for CaO showed peaks at $18.14^\circ, 28.73^\circ, 34.16^\circ, 47.11^\circ, 50.86^\circ, 54.36^\circ, 62.76^\circ, 64.41^\circ, 72.05^\circ, \text{ and } 84.87^\circ$ which confirmed the presence of CaO phase.⁽⁴¹⁾ The cubic phase of CeO_2 as confirmed by the presence of the characteristic peaks observed at $2\theta = 28.83^\circ, 33.2^\circ, 47.9^\circ, 56.7^\circ$ and 59.4° corresponding to (111), (200), (220), (311) and (222) planes, respectively.⁽⁴²⁾ The XRD pattern for Al_2O_3 showed weak diffraction peaks, observed at $2\theta = 19.2^\circ, 31.0^\circ, 36.6^\circ, 39.3^\circ, 46^\circ, 61.5^\circ, \text{ and } 67^\circ$, which can be indexed to the reflections at (111), (220), (311), (222), (400), (511), and (440) corresponding to the presence of γ -alumina phase according to JCPDS card: 100425.⁽⁴³⁾ The detailed morphology, surface topography of the catalysts was studied FE- SEM.

Figure 2 displays the SEM images for various catalysts, in different magnifications *viz.* (a) CaO, (b) BaO, (c) La₂O₃, (d) Ce₂O₃. In case of calcined La₂O₃, irregular and uneven shaped particles were predominantly present as shown in Fig. 2c. The SEM images clearly indicated the presence of pores of varied sizes in the range 90–450 nm on the surface. The presence of these nano pores aid in providing high surface area for adsorption. The SEM analysis of cerium oxide is shown in Fig. 2d. The morphological investigation revealed the presence of pores with spherical shaped particles distributed on the surface with size 90–420 nm. BaO showed the presence of mixed morphology with spherical and rod shaped particles. Rod shaped particles were present predominantly with length in the range of 1–2.8 μm and the size of the spherical particles in the range 220–450 nm as shown in Fig. 2b.⁽⁴⁰⁾ In case of CaO as shown in Fig. 2a, the morphology revealed to contain clusters of flakey particles with particle size, *viz.* 150–750 nm. The percentage elemental composition was acquired by EDS analysis for all four metal oxide catalysts screened (Supporting information **Fig.sS-10, S-11, S-12, S-13**). It confirmed the presence of La₂O₃ phase having composition in mass percentage of the elements as 39.69% O and 60.31% La by weight. The peak indexing of the elements for lanthanum was 4.63 KeV and for oxygen was 0.51 KeV.

High Resolution-Transmission Electron Microscopy (HR-TEM) was utilized for detailed study of the size, shape, morphology and surface distribution of the particles as shown in Fig. 3. Irregular, unordered distributions of the particles were observed at the surface. The agglomeration of the nano particles due to aggregation of the particles by weak forces was observed with average pore size in the range 90–500 nm.⁽⁴⁴⁾ Thus, from the HR-TEM characterization we conclude that the agglomerated catalyst possess good porosity due to the presence of pores in the nano range.⁽⁴⁵⁾

Figure 4A presents FT-IR spectra of calcined (La₂O₃) in the range 400–4000 cm⁻¹ which showed detailed information about the metal and oxygen bond present in the metal oxide catalysts. The FTIR spectrum of La₂O₃ sample showed a prominent band at 637 cm⁻¹ which was assigned to the stretching vibration of La-O. The intense and sharp absorption band at 3619 cm⁻¹ was ascribed to the -OH stretching of water molecule adsorbed from atmosphere on the oxide surface and the band at 1530 cm⁻¹ corresponds to the presence of extending and twisting -OH bending vibration due to the physically adsorbed water molecule on the catalyst surface. This confirms the presence of Brønsted basic sites in the form of La(OH)₃ phase.^(46–48) Hence, the appearance of the above mentioned bands in the FTIR spectra confirmed the presence of La₂O₃ and the La(OH)₃ phases in accordance with XRD study.⁽⁴⁹⁾ BaO showed an intense band at 692 cm⁻¹ corresponding to Ba-O stretching frequency. Whereas, the band at 512 cm⁻¹ was assigned to the Ca-O stretching vibration. The Ce-O stretching frequency was observed at 613 cm⁻¹. In case of CaO and BaO, the absorption band due to the bending vibration of the adsorbed water molecule on the catalyst surface was observed at 1448 cm⁻¹ and intense and sharp absorption due to the -OH stretching of the adsorbed water molecule was observed at 3645 cm⁻¹ (sharp) and 3350–3655 cm⁻¹ (broad). The broad absorption band corresponds to the superposition of the hydroxyl stretching bands due to the hydroxyl groups present at the metal oxide surface and the hydrogen bond. But in Ce₂O₃, the band due to bending vibration for the adsorbed water molecule shifted to 1626 cm⁻¹ and a broad absorption band at 3200–3650 cm⁻¹ was observed due to adsorbed water molecule at the catalytic surface. This clearly indicates the presence of hydroxyl group on the catalytic surface.

Figure 4B represents the in-situ FT-IR spectra obtained by subtracting adsorbed MeOH on metal oxide and neat metal oxide spectra. The investigation of Brønsted basicity was carried out by performing in-situ methanol adsorption-IR spectroscopy. Earlier, Verneker et al. studied various interactions of FeO(OH) at the surface by MeOH adsorption IR spectroscopy. Their results showed that MeOH interacts with the basic sites on the catalytic surface to form monodentate methoxy species, bidentate methoxy species and molecularly adsorbed species with bands observed at 1115 cm⁻¹, 1092 cm⁻¹, 1064 cm⁻¹.^(50–52) In Fig. 4B, various interactions of the adsorbed MeOH with the catalytic

surface can be seen. The formation of H-bonded molecularly adsorbed MeOH at the La_2O_3 surface was observed with a band at 1064 cm^{-1} . Whereas, the bands at 1115 cm^{-1} and 1092 cm^{-1} indicated the formation of monodentate and bidentate methoxy species/ metal complexed methoxy species. All these bands were observed in La_2O_3 , Ce_2O_3 , CaO and BaO catalysts. The La_2O_3 catalyst showed intense band at 1063 cm^{-1} and 1117 cm^{-1} whereas, CaO and BaO showed weak bands in this region. The presence of these intense bands in La_2O_3 catalyst clearly indicates the presence of Brønsted basic sites on the catalyst surface, which play an important role in the NAG dehydration.

Table 1 reveals the physico chemical properties of the screened catalysts. The surface areas of the catalysts determined by the Brunauer–Emmett–Teller (BET) measurement using N_2 adsorption-desorption isotherms, were found to be $98.097\text{ m}^2\text{g}^{-1}$ for calcium oxide, $8.073\text{ m}^2\text{g}^{-1}$ for barium oxide, $12.186\text{ m}^2\text{g}^{-1}$ for lanthanum oxide and $13.294\text{ m}^2\text{g}^{-1}$ for cerium oxide catalyst. Fig.S-8 (supporting info.) represents the adsorption isotherm of all the catalysts. The N_2 adsorption-desorption isotherm gives detailed information of surface area, pore volume and pore size of the catalyst calculated using BJH method. The La_2O_3 catalyst exhibited adsorption isotherm which represents unrestricted multilayer formation due to strong lateral interactions between the adsorbed molecules.⁽⁵³⁾ The steepness of the isotherm was found to decrease in the order $\text{BaO} > \text{CaO} > \text{La}_2\text{O}_3 = \text{Ce}_2\text{O}_3$. The hysteresis loop in case of CaO showed the presence of relatively uniform and narrow pores whereas, the hysteresis loop for La_2O_3 and Ce_2O_3 showed the presence of narrow pores with irregular shape and size.^(54–55) Table 1 shows the BET surface area in terms of (m^2g^{-1}), it showed the total surface area of $12.186\text{ m}^2/\text{g}$, pore volume of 0.0413 cc/g and pore diameter of 0.1357 nm .^(56–57) whereas, Ce_2O_3 showed total surface area of $13.294\text{ m}^2\text{g}^{-1}$, pore volume of 0.0405 ccg^{-1} and pore diameter of 0.1219 nm . Also, BaO and CaO exhibited total surface area of $8.073\text{ m}^2/\text{g}$ and $98.097\text{ m}^2/\text{g}$, pore volume of 0.0132 cc/g and 0.1569 cc/g and pore diameter of 0.6582 nm and 0.6398 nm respectively.

Table 1 showed the total CO_2 desorbed in terms of mmol/gm as well as the temperature wise distribution of the basic sites at the catalytic surface for all the samples under study. It was used to determine the surface basicity of the catalytic samples. The catalytic samples exhibited three CO_2 desorption peaks corresponding to the weak, moderate and strong Brønsted basicity. The first peak in the region of $100\text{--}200\text{ }^\circ\text{C}$ represents weak Brønsted basicity corresponding to the desorption of physisorbed CO_2 . Whereas, the peak in the temperature range $200\text{--}400\text{ }^\circ\text{C}$ represents moderate basic strength and that in the range $400\text{--}700\text{ }^\circ\text{C}$ represents strong basicity. The orders of the total basicity of the screened catalysts were found to be $\text{BaO} > \text{CaO} > \text{La}_2\text{O}_3 > \text{Ce}_2\text{O}_3$. The total basicity of La_2O_3 was $0.3854\text{ mmol g}^{-1}$, $0.0867\text{ mmol g}^{-1}$ for Ce_2O_3 , $0.7533\text{ mmol g}^{-1}$ for CaO and highest $0.99110\text{ mmol g}^{-1}$ for BaO catalyst. Fig.S9 (supporting info.) represents the TPD plots for various screened catalysts. The La_2O_3 catalyst was found to give total basicity around $0.3854\text{ mmol g}^{-1}$ with peak maxima at $335\text{ }^\circ\text{C}$. Whereas, CaO was found to give basicity of $0.7533\text{ mmol g}^{-1}$ with peak maxima at $420\text{ }^\circ\text{C}$, Cerium oxide showed basicity of $0.0867\text{ mmol g}^{-1}$ with peak maxima at $290\text{ }^\circ\text{C}$ and BaO showed highest basicity of $0.9911\text{ mmol g}^{-1}$. The CaO and BaO showed maximum desorption in the higher temperature range. Whereas, La_2O_3 and Ce_2O_3 catalyst showed maximum desorption in the medium temperature range. This was due to the $-\text{OH}$ moiety at the catalytic surface and the presence of co-ordinated O^{2-} species as evidenced by the MeOH-FTIR (presence of Brønsted sites) and XRD analysis (presence of $\text{La}(\text{OH})_3$ phase). As, La_2O_3 catalyst showed strong desorption peak in the low temperature range than Ce_2O_3 catalyst, indicating the presence of weak but dense basic sites at the catalytic surface amongst all the catalysts. Hence, the basic properties of the metal oxide catalyst were evaluated quantitatively by CO_2 -TPD measurement.

Table 1
Physico-chemical properties of the catalysts

Sr. No.	Catalyst	S-[BET] ^a (m ² g ⁻¹)	Pore volume ^b (cc g ⁻¹)	Pore diameter ^b (nm)	Distribution of basic sites (mmolg ⁻¹)			Total Basicity ^c (total CO ₂ desorbed, mmol g ⁻¹)
					Temperature ^c (°C) (100–200)	Temperature ^c (°C) (200–400)	Temperature ^c (°C) (400–700)	
1	CaO	98.097	0.1569	0.6398	-	0.6780	0.0753	0.7533
2	BaO	8.073	0.0132	0.6582	0.0081	0.8512	0.1318	0.9911
3	La ₂ O ₃	12.186	0.0413	0.1357	0.2739	0.0940	0.0175	0.3854
4	Ce ₂ O ₃	13.294	0.0405	0.1219	0.0090	0.0068	0.0709	0.0867

a- BET analysis, b- BJH method, c-Determined by CO₂ TPD measurement, S-[BET] - BET surface area

3.2 Catalyst Screening

One pot partial deoxygenation and dehydration of NAG to 3AF and 3A5AF was studied using various metal oxides and the results are presented in Table 2. NAG in absence of any catalyst under the same reaction conditions didn't show any formation of 3AF and 3A5AF. Interestingly, all the metal oxides showed activities according to acidic and basic nature, they possessed. Al₂O₃ catalyst gave 11% yield of 3AF and 18% yield towards 3A5AF (Table 2, **entry 1**). For ZrO₂ as a catalyst, NAG yields 12% of 3AF and 6% of 3A5AF (Table 2, **entry 2**). BaO showed 19% and 5% yield for 3AF and 3A5AF, respectively (Table 2, **entry 3**). CaO produced 36% yield of 3AF and 19% yield towards 3A5AF (Table 2, **entry 4**). It can be seen that the basic nature of the catalyst is responsible for formation of the desired product i.e. 3AF as compared to activities shown by acidic metal oxides. The 3AF yield could be enhanced by using rare earth metal oxides which possess appreciable basic characteristics. La₂O₃ showed almost complete conversion of NAG with 50% yield towards 3AF and 21% yield for 3A5AF (Table 2, **entry 5**). Another lanthanum series metal oxide Ce₂O₃ gave 32% 3AF yield and 11% yield for 3A5AF (Table 2, **entry 6**). It can be inferred from the above results that La₂O₃ was a very promising catalyst for NAG dehydration and partial deoxygenation producing 3AF product more selectively. La₂O₃ showed better yield for 3AF as it possesses moderate basicity which are Brønsted in nature along with well distributed three-dimensional interconnected nanopores which can be clearly seen from HR-TEM micrographs. These nanopores present on the surface of La₂O₃ play a very important role during reaction, allowing improved diffusion of reactants and products. Further using La₂O₃ as catalyst optimization of various reaction parameters was carried out for achieving the maximum yield for desired 3AF product.

Table 2
Catalyst screening for NAG conversion to 3AF and 3A5AF

Sr. No.	Catalyst	Yield (%)	
		3AF	3A5AF
1	Al ₂ O ₃	11	18
2	ZrO ₂	12	06
3	BaO	19	05
4	CaO	36	19
5	La ₂ O ₃	50	21
6	Ce ₂ O ₃	32	11
Reaction Condition: NAG (1 gm), catalyst (0.2 gm), Dioxane (25 mL), temperature, 180 °C; reaction time, 3 h			

3.2.1 Effect Of Substrate To Catalyst Ratio

Figure 5 represents the effect of substrate to catalyst ratio on N-acetyl-glucosamine conversion. The catalyst loading was varied in range 5 to 25 wt. % with respect to the substrate (constant at 1 gm) to determine its effect on NAG conversion to 3AF. With increase in the catalyst loading from 5 to 20 wt. % there was an increase in the yield from 20 to 50%, which could be imputed to the availability of nanopores as well as active basic sites at the catalytic surface for better adsorption. As the catalyst loading was further increased to 25 wt. % there was slight decrease in the yield (48%), due to increase in the formation of humins. Thus, 20 wt. % of the catalyst was optimized for desired conversion.

3.2.1 Effect Of Time

Figure 6 shows significant increase in 3AF and 3A5AF production with increase in time 60 to 180 min. 3AF and 3A5AF yields were found to increase linearly with increase in time to maximum upto 50% and 19%, respectively. However, the yield of 3AF and 3A5AF was found to decrease after 180 min due to thermal decomposition of the products and acceleration in the rate of formation of humins as by-product was favoured by elevated temperature and prolonged time.

3.2.3 Effect Of Reaction Temperature

Figure 7 shows the effect of temperature on N-acetyl glucosamine conversion. NAG conversion to 3AF with La₂O₃ catalyst was studied by examining the reaction at various temperatures in range 120–210 °C. Figure 8 illustrates that with increase in temperature there was a linear increase in the yield of 3AF and reached to maximum at 180 °C. With further increase in the temperature to 210 °C, the product yield decreased as high temperature accelerated the humin formation. Thus, with increase in temperature above 180 °C, the selectivity to 3AF decreased due to enhancement in the formation of humins. Thus, this decrease in product yield at elevated temperature (above 180 °C) indicates that high temperature favours humin formation. The increase in temperature causes heat transfer resulting in increase in collisions between the particles thereby increasing the collision frequency. This lowers the energy of activation and

enhances the reaction rates. The increasing temperature accelerated the 3AF production. Thus, maximum 50% 3AF yield was observed within 3 h at 180 °C.

3.2.4 Solvent Screening

Solvents play a vital role in various phenomena such as heat transfer, providing medium for reaction, separation and purification of the products. Figure 8 exhibits the effect of solvent on N-acetyl glucosamine conversion to 3AF. In order to understand the influence of solvent system on NAG conversion to 3AF and 3A5AF, several solvents such as DMA, DMSO, DMF, MIBK and dioxane were screened. DMA, DMSO and DMF were preferred solvents as they were used for dehydration of cellulosic and chitin biomass previously.⁽⁵⁸⁾ Whereas, dioxane is an aprotic solvent and is able to solvate various inorganic compounds in it. DMF gave highest product yield of 55%, while DMA, DMSO, MIBK and dioxane gave 52%, 48%, 39% and 50% yields of 3AF, respectively. Among these, DMF, DMA and DMSO are toxic and have few health hazards and separation of products is quite tedious as these are high boiling solvents. Also, MIBK showed low selectivity to the product due to formation of large amount of humins. Thus, dioxane was chosen as the best solvent for this conversion.

3.2.5 Effect Of Addition Of Water On Reaction Pathway:

As water being green solvent and chitin biomass being readily soluble in water, the mixtures of above individual solvents with water were screened for the conversion of NAG to 3 AF and 3A5AF. It was observed that the addition of water to the organic phase significantly decreased the product selectivity. Thus, the addition of water to the organic phase showed negative effect on the product yield and selectivity. This could be attributed to the fact that water caused acceleration in the formation of humins thereby decreasing the selectivity of the product formation. The effect of addition of water on NAG conversion was studied by adding 50% water to the solvent system chosen. Figure 9 shows the effect of addition of water to the solvents DMA, DMSO, DMF, MIBK and Dioxane on N-Acetylglucosamine conversion. Thus, water has negative effect on NAG conversion as presence of water enhances the humin formation.

3.2.6 Catalyst Recycle Study

The recycle study of the heterogeneous (La_2O_3) catalyst was carried out under the optimized conditions and results are as shown in Fig. 10. After the first run, catalyst was filtered and washed with deionised water till the pale-yellow coloured catalyst faded, the catalyst was dried at 110 °C in an oven and then calcined at 550 °C for further 3 runs. The procedure was followed for four successive cycles. The N-acetyl glucosamine conversion decreased by marginally by 3% (from 50–47%) due to handling losses. In order to study the changes of the catalyst surface during the reaction, the recovered catalyst was characterised by XRD, FTIR and TGA analysis. The XRD pattern of the used catalyst (Fig. 11) showed that the crystallinity of the catalyst remained intact and there was no deposition of any carbonatious material at the catalytic surface. The FTIR spectrum of the reused catalyst (Fig. 12) was similar with that of the fresh catalyst which confirms the stability of the catalyst. The TGA analysis (Fig.S-14, supporting info.) of the catalysts confirmed that the catalyst was thermally stable. Thus, the La_2O_3 catalyst showed exquisite recyclability performance up to 4 cycles.

Plausible Mechanism

The N-Acetyl glucosamine undergoes ring opening in the presence of basic sites of the catalyst to form an open chain compound as shown in **Scheme I, route A**. The presence of nano pores on the catalyst surface as confirmed by SEM and HR-TEM analysis are found to play vital role in the adsorption of the substrate molecules. The basic sites of the catalyst participate in the abstraction of C4-OH proton (I). The nucleophilic attack of C4-O on C1-carbonyl (I) results in the formation of five membered cyclic ring (II) predominantly as formation of five membered ring is favored. This (II) further undergoes dehydration followed by elimination of CH₂OHCHO moiety. The driving force for elimination and dehydration is aromatization which provides extra stability to the system thereby forming 3-acetamido furan (III) as the major product with 50% yield. Whereas, 3A5AF (VI) is formed as a minor product with 21% yield as shown in **Scheme I, route B**, which is formed by nucleophilic attack of C4-OH on C1-carbonyl (I) results in the formation of five member cyclic ring (IV). This is followed by dehydration with removal of two water molecules, as it makes the system more stable due to aromatization (V) which on keto-enol tautomerism results in the formation of 3A5AF (VI) with 21% yield.⁽¹⁶⁾ The insoluble polymer humins are also formed as byproduct during the course of the reaction. Both the products formed were extracted by using a mixture of ethyl acetate and water followed by its purification by column chromatography using 50% ethyl acetate and n-hexane as the mobile phase. The products formed were confirmed by ¹H-NMR, ¹³C-NMR, HRMS and FTIR (NAG and 3AF, 3A5AF) analysis qualitatively (supporting information **Fig.sS-1a, S-1b, S-2a, S-2b, S-3 and S-4, S-5, S-6**). The NAG conversion was quantitatively determined by HPLC analysis by keeping 0.5 mL/min flow rate of the prepared mobile phase maintaining column temperature at 80 °C and total analysis time of 20 minutes. The calibration curve is given in supplementary material. **Fig.S7** which showed complete conversion of NAG (supporting information).

Conclusion

A comparative study of various metal oxide catalysts such as La₂O₃, Ce₂O₃, Al₂O₃, ZrO₂, BaO and CaO was undertaken for the dehydration of N-acetyl glucosamine to render important furanic compounds. The physico-chemical properties of the catalyst were studied by XRD, CO₂-TPD, BET surface area measurements, SEM, HR-TEM, MeOH- FTIR analysis. The parameters such as solvent, temperature, time and substrate concentration were optimized for efficient catalytic activity. Various experiments carried out with organic solvents and their mixtures with water revealed that dioxane was the best solvent for NAG conversion whereas, water was found to inhibit the reaction thereby accelerating the formation of humins. La₂O₃ excel as catalyst for the transformation of N-Acetylglucosamine which yields 50% 3AF and 19% 3A5AF at 180 °C in 3h. The superior performance was attributed to the presence of moderate basicity which was Brønsted in nature as confirmed from MeOH-FTIR originating from presence of La(OH)₃. While, FE-SEM, and HR-TEM disclosed existence of nanopores on the catalytic surface. The cooperative effect of Brønsted basicity and nanopores (90–450 nm) were found to play important role in NAG conversion to N-containing platform molecules. We reported for the first time the use of heterogeneous catalyst La₂O₃ to produce 50% 3AF and 21% 3A5AF yield which was 10 times more than the yield reported by the pyrolysis method. The catalyst was recyclable upto 4 cycles and easily separable. As far as sustainability is concerned this study represents a direct one pot conversion of NAG to N-substituted renewable compounds by valorization of marine biomass.

Abbreviations

DMSO, dimethyl sulfoxide; GlcNAc, N-Acetyl-D-glucosamine; GlcNH₂, glucosamine; HMF, 5-hydroxymethylfurfural; IL, ionic liquid; LA, levulinic acid; NAG, N-Acetyl-D-glucosamine; EtOAc; Ethylacetate, DMA, Dimethylacetamide; DMF, Dimethylformamide; MIBK, Methylisobutylketone; 3AF, 3-acetamido furan; 3A5AF, 3-acetamido-5-acetyl furan; 3A5HEF, 3-Acetamido-5-(1-hydroxyethyl)furan.

Declarations

Conflict of interest

The authors declare that they have no conflict of interests.

Author Contributions

The first draft of the manuscript was written by Samrin Shaikh. S and all authors commented on previous versions of the manuscript. All authors read and approved the final manuscript. Samrin Shaikh. S, Conceptualization, Data analysis, Investigation, Methodology, Writing, Chetana. R. Patil, Writing, Dr. V. V. Bokade, supervision, Nishita. Lucas, writing and Dr. C. V. Rode, Conceptualization, Supervision and Writing.

Acknowledgement

Samrin S. Shaikh acknowledges Council of Scientific & Industrial Research (CSIR) for providing financial support, reference no. 21(1054)/18/EMR-II and AcSIR for providing various facilities to carry out the research work successfully. One of the authors, Chetana R. Patil acknowledge Council of Scientific & Industrial Research (CSIR), for the award of Research Associateship vide reference no. 31/011(1141)/2020-EMR-I for the financial assistance to carry out this work.

AUTHOR INFORMATION

*Corresponding Author

CSIR-National Chemical Laboratory, Dr. HomiBhaba Road, Pune 411008, India.

Email: cv.rode@ncl.res.in, cvrode8@gmail.com, Tel.: +91 (020) 25902349

References

1. Nel, W.P., Cooper, C.J.: Implications of fossil fuel constraints on economic growth and global warming. *Energy Policy*. **37**, 166–180 (2009)
2. Shafiee, S., Topal, E.: When will fossil fuel reserves be diminished? *Energy policy*. **37**, 1, 181–189 (2009)
3. Arancon, R.A.D., Lin, C.S.K., Chan, K.M., Kwan, T.H.: Luque, R. Advances on waste valorization: new horizons for a more sustainable society. In *Waste Management and Valorization* Apple Academic Press. 23–66 (2017)
4. Hülsey, M.J., Yang, H.: Yan, N. Sustainable routes for the synthesis of renewable heteroatom-containing chemicals. *ACS Sustain. Chem. Eng.* **6**, 5, 5694–5707 (2018)
5. Hussain, A., Arif, S.M., Aslam, M.: Emerging renewable and sustainable energy technologies: State of the art. *Renew. Sustain. Energy Rev.* **71**, 12–28 (2018)
6. Gooday, G.W.: The ecology of chitin degradation. In *Advances in microbial ecology*. Springer, Boston, MA. 387–430 (1990)
7. Yan, N., Chen, X., Sustainability: Don't waste seafood waste. *Nature*. **524**, 7564, 155–157 (2015)
8. Chen, X., Yang, H., Yan, N.: Shell biorefinery: dream or reality? *Chem. Eur. J.* **22**, 38, 13402–13421 (2016)

9. Chen, X., Liu, Y., Wang, J.: Lignocellulosic biomass upgrading into valuable nitrogen-containing compounds by heterogeneous catalysts. *Ind. Eng. Chem. Res.* **59**, 39, 17008–17025 (2020)
10. Chen, X., Song, S., Li, H., Gözaydın, G., Yan, N.: Expanding the boundary of biorefinery: organonitrogen chemicals from biomass. *Acc. Chem. Res.* **54**, 7, 1711–1722 (2021)
11. Lucas, N., Athawale, A.A., Rode, C.V.: Valorization of oceanic waste biomass: a catalytic perspective. *Chem. Rec.* **19**, 9, 1995–2021 (2019)
12. Elieh-Ali-Komi, D., Hamblin, M.R.: Chitin and chitosan: production and application of versatile biomedical nanomaterials. *Int. J. Adv. Res. Publ.* **4**, 3, 411 (2016)
13. Khoushab, F., Yamabhai, M.: Chitin research revisited. *Mar. Drugs.* **8**, 7, 1988–2012 (2010)
14. Younes, I., Rinaudo, M.: Chitin and chitosan preparation from marine sources. Structure, properties and applications. *Mar. Drugs.* **13**, 3, 1133–1174 (2015)
15. Raafat, D., Sahl, H.G.: Chitosan and its antimicrobial potential—a critical literature survey. *Microb. Biotechnol.* **2**, 2, 186–201 (2009)
16. Chen, J., Wang, M., Ho, C.T.: Volatile compounds generated from thermal degradation of N-acetylglucosamine. *J. Agric. Food Chem.* **46**, 8, 3207–3209 (1998)
17. Omari, K.W., Dodot, L., Kerton, F.M.: A simple one pot dehydration process to convert N-acetyl D-glucosamine into a nitrogen containing compound, 3-acetamido-5-acetylfuran. *ChemSusChem.* **5**, 9, 1767–1772 (2012)
18. Drover, M.W., Omari, K.W., Murphy, J.N., Kerton, F.M.: Formation of a renewable amide, 3-acetamido-5-acetylfuran, via direct conversion of N-acetyl-d-glucosamine. *Rsc Adv.* **2**, 11, 4642–4644 (2012)
19. Chen, X., Chew, S.L., Kerton, F.M., Yan, N.: Direct conversion of chitin into a N-containing furan derivative. *Green. Chem.* **16**, 4, 2204–2212 (2014)
20. Franich, R.A., Goodin, S.J., Wilkins, A.L.: Acetamidofurans, acetamidopyrones, and acetamidoacetaldehyde from pyrolysis of chitin and n-acetylglucosamine. *J. Anal. Appl. Pyrolysis.* **7**(1–2), 91–100 (1984)
21. Omari, K.W., Dodot, L., Kerton, F.M.: A simple one pot dehydration process to convert N-acetyl D glucosamine into a nitrogen containing compound, 3-acetamido 5 acetylfuran. *ChemSusChem.* **5**, 9, 1767–1772 (2012)
22. Sadiq, A.D., Chen, X., Yan, N., Sperry, J.: Towards the shell biorefinery: sustainable synthesis of the anticancer alkaloid proximicin A from chitin. *ChemSusChem.* **11**, 3, 532–535 (2018)
23. Bobbink, F.D., Zhang, J., Pierson, Y., Chen, X., Yan, N.: Conversion of chitin derived N-acetyl-d-glucosamine (NAG) into polyols over transition metal catalysts and hydrogen in water. *Green. Chem.* **17**(2), 1024–1031 (2015)
24. Dai, J., Li, F., Fu, X.: Towards Shell Biorefinery. *Advances in Chemical Catalytic Conversion of Chitin Biomass to Organonitrogen Chemicals.* *ChemSusChem.* **13**, 24, 6498–6508 (2020)
25. Pham, T.T., Chen, X., Yan, N., Sperry, J.: A novel dihydrodifuro-pyridine scaffold derived from ketones and the chitin-derived heterocycle 3-acetamido-5-acetylfuran. *Monatshefte für Chemie-Chemical Monthly.* **149**(4), 857–861 (2018)
26. Lindsay, T.T., Kim, A.C., Persello, S.W., Chen, L., Yan, X., Sperry, N.: Two Step Preparation of Diverse 3-Amidofurans from Chitin. *ChemistrySelect.* **4**, 34, 10097–10099 (2019)
27. Xin, Y., Shen, X., Liu, H., Han, B.: Selective Utilization of N-acetyl Groups in Chitin for Transamidation of Amines. *Front. ChemSci Eng.* **2**, 634983 (2021)
28. Pham, T.T., Chen, X., Söhnel, T., Yan, N., Sperry, J.: Haber-independent, diversity-oriented synthesis of nitrogen compounds from biorenewable chitin. *Green. Chem.* **22**(6), 1978–1984 (2020)

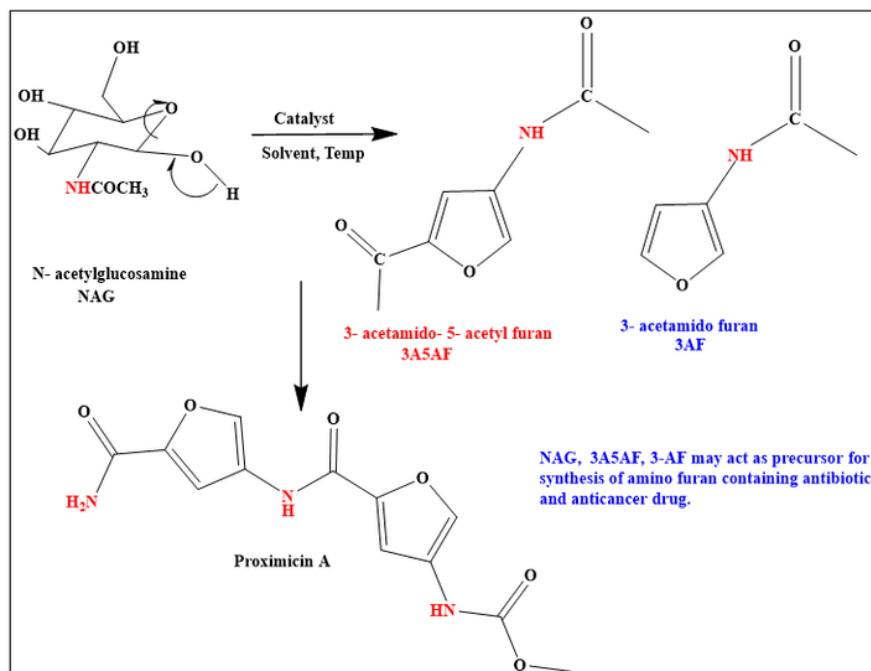
29. Johdo, O., Yoshioka, T., Naganawa, H., Takeuchi, T., Yoshimoto, A.: New betaclamycin and aclarubicin analogs obtained by prolonged microbial conversion with an aclarubicin-negative mutant. *J. Antibiot.* **49**, 7, 669–675 (1996)
30. Shaaban, K.A., Ahmed, T.A., Leggas, M., Rohr, J.: Saquayamycins G–K, cytotoxic angucyclines from *Streptomyces* sp. including two analogues bearing the aminosugarrednose. *J. Nat. Prod.* **75**, 7, 1383–1392 (2012)
31. Doyle, T.W., Nettleton, D.E., Grulich, R.E., Balitz, D.M., Johnson, D.L., Vulcano, A.L.: Antitumor agents from the bohemiacid complex. 4. Structures of rudolphomycin, mimimycin, collinemycin, and alcindoromycin. *J. Am. Chem. Soc.* **101**, 23, 7041–7049 (1979)
32. Hao, Y.C., Zong, M.H., Wang, Z.L., Li, N.: Chemoenzymatic access to enantiopure N-containing furfuryl alcohol from chitin-derived N-acetyl-D-glucosamine. *Bioresour Bioprocess.* **8**(1), 1–9 (2021)
33. Drover, M.W., Omari, K.W., Murphy, J.N., Kerton, F.M.: Formation of a renewable amide, 3-acetamido-5-acetylfuran, via direct conversion of N-acetyl-d-glucosamine. *Rsc Adv.* **2**, 11, 4642–4644 (2012)
34. Chen, X., Chew, S.L., Kerton, F.M., Yan, N.: Direct conversion of chitin into a N-containing furan derivative. *Green. Chem.* **16**, 4, 2204–2212 (2014)
35. Wang, J., Zang, H., Jiao, S., Wang, K., Shang, Z., Li, H., Lou, J.: Efficient conversion of N-acetyl-d-glucosamine into nitrogen-containing compound 3-acetamido-5-acetylfuran using amino acid ionic liquid as the recyclable catalyst. *Sci. Total Environ.* **710**, 136293 (2020)
36. Qi, X., Watanabe, M., Aida, T.M., Smith, R.L. Jr.: Efficient one-pot production of 5-hydroxymethylfurfural from inulin in ionic liquids. *Green. Chem.* **12**, 10, 1855–1860 (2010)
37. Khalaf, W.M., Al-Mashhadani, M.H.: Synthesis and Characterization of Lanthanum Oxide La_2O_3 Net-like Nanoparticles by New Combustion Method. *Biointerface Res. Appl. Chem.* **12**, 3066–3075 (2022)
38. Singh, A., Palakollu, V., Pandey, A., Kanvah, S., Sharma, S.: Green synthesis of 1, 4-benzodiazepines over La_2O_3 and $\text{La}(\text{OH})_3$ catalysts: Possibility of Langmuir–Hinshelwood adsorption. *RSC Adv.* **6**, 105, 103455–103462 (2016)
39. Li, S.C., Hu, S.J., Du, N., Fan, J.N., Xu, L.J., Xu, J.: Low-temperature chemical solution synthesis of dendrite-like $\text{La}(\text{OH})_3$ nanostructures and their thermal conversion to La_2O_3 nanostructures. *Rare Met.* **34**, 395–399 (2015)
40. Shaikh, S.S., Patil, C.R., Kondawar, S.E., Rode, C.V.: Cooperative Acid Base Sites of Solid BaZr Mixed Oxide Catalyst for Efficient Isomerization of Glucose to Fructose in Aqueous Medium. *ChemistrySelect.* **5**, **40**, 12505–12513 (2020)
41. Yazıcılar, B., Böke, F., Alaylı, A., Nadaroglu, H., Gedikli, S., Bezirganoglu, I.: In vitro effects of CaO nanoparticles on Triticale callus exposed to short and long-term salt stress. *Plant. Cell. Rep.* **40**(1), 29–42 (2021)
42. Peng, S., Sun, X., Sun, L., Zhang, M., Zheng, Y., Su, H., Qi, C.: Selective hydrogenation of acetylene over gold nanoparticles supported on CeO_2 pretreated under different atmospheres. *Catal. Lett.* **149**, 2, 465–472 (2019)
43. Romero Toledo, R., RuízSantoyo, V., Moncada Sánchez, D., Martínez Rosales, M.: Effect of aluminum precursor on physicochemical properties of Al_2O_3 by hydrolysis/precipitation method. *Nova scientia.* **10**, 20, 83–99 (2018)
44. Matsouka, V., Konsolakis, M., Lambert, R.M., Yentekakis, I.V.: In situ DRIFTS study of the effect of structure (CeO_2 – La_2O_3) and surface (Na) modifiers on the catalytic and surface behaviour of $\text{Pt}/\gamma\text{-Al}_2\text{O}_3$ catalyst under simulated exhaust conditions. *Appl. Catal. B: Environ.* **84**(3–4), 715–722 (2008)
45. Tejani, J., Shah, R., Vaghela, H., Vajapara, S., Pathan, A.: Controlled Synthesis and Characterization of Lanthanum Nanorods. *Int. J. Thin Film Sci. Technol.* **9**, 2, 5 (2020)

46. Verma, N.K.: Study on the controlled growth of lanthanum hydroxide and manganese oxidenano composite under the presence of cationic surfactant. *Adv. Mater.* **4**, 11–15 (2015)
47. Mu, Q., Wang, Y.: Synthesis, characterization, shape-preserved transformation, and optical properties of La (OH)₃, La₂O₂CO₃, and La₂O₃nanorods. *J. Alloys Compd.* **509**, 2, 396–401 (2011)
48. Zhu, H., Yang, D., Yang, H., Zhu, L., Li, D., Jin, D., Yao, K.: Reductive hydrothermal synthesis of La(OH)₃: Tb³⁺nanorods as a new green emitting phosphor. *J. Nanoparticle Res.* **10**, 2, 307–312 (2008)
49. Fleming, P., Farrell, R.A., Holmes, J.D., Morris, M.A.: The rapid formation of La (OH)₃ from La₂O₃ powders on exposure to water vapor. *J. Am. Ceram. Soc.* **93**(4), 1187–1194 (2010)
50. Vernekar, D., Sakate, S.S., Rode, C.V., Jagadeesan, D.: Water-promoted surface basicity in FeO (OH) for the synthesis of pseudoionones (PS) and their analogues. *J. Catal.* **378**, 80–89 (2019)
51. Bailly, M.L., Chizallet, C., Costentin, G., Krafft, J.M., Lauron-Pernot, H., Che, M.: A spectroscopy and catalysis study of the nature of active sites of MgO catalysts: Thermodynamic Brønsted basicity versus reactivity of basic sites. *J. Catal.* **235**, 2, 413–422 (2005)
52. Bensitel, M., Saur, O., Lavalley, J.C.: Use of methanol as a probe to study the adsorption sites of different MgO samples. *Mater. Chem. Phys.* **28**, 3, 309–320 (1991)
53. Li, Y., Lin, J., Wang, G.: La₂O₃/Fe₂O₃-CeO₂ Composite Oxide Catalyst and Its Performance. *Adv. Mater. Phys. Chem.* **9**, 12, 219–233 (2019)
54. Othman, A.L.: A review: fundamental aspects of silicate mesoporous materials. *Materials.* **5**, 12, 2874–2902 (2012)
55. Uppal, S., Arora, A., Gautam, S., Singh, S., Choudhary, R.J., Mehta, S.K.: Magnetically retrievable Ce-doped Fe₃O₄ nanoparticles as scaffolds for the removal of azo dyes. *RSC adv.* **9**, 40, 23129–23141 (2019)
56. Adole, V.A., Pawar, T.B., Koli, P.B., Jagdale, B.S.: Exploration of catalytic performance of nano-La₂O₃ as an efficient catalyst for dihydropyrimidinone/thione synthesis and gas sensing. *J. Nanostructure Chem.* **9**(1), 61–76 (2019)
57. Ambroz, F., Macdonald, T.J., Martis, V., Parkin, I.P.: Evaluation of the BET Theory for the Characterization of Meso and Microporous MOFs. *Small methods.* **2**, 11, 1800173 (2018)
58. Zang, H., Lou, J., Jiao, S., Li, H., Du, Y., Wang, J.: Valorization of chitin derived N-acetyl-D-glucosamine into high valuable N-containing 3-acetamido-5-acetylfuran using pyridinium-based ionic liquids. *J. Mol. Liq.* **330**, 115667 (2021)

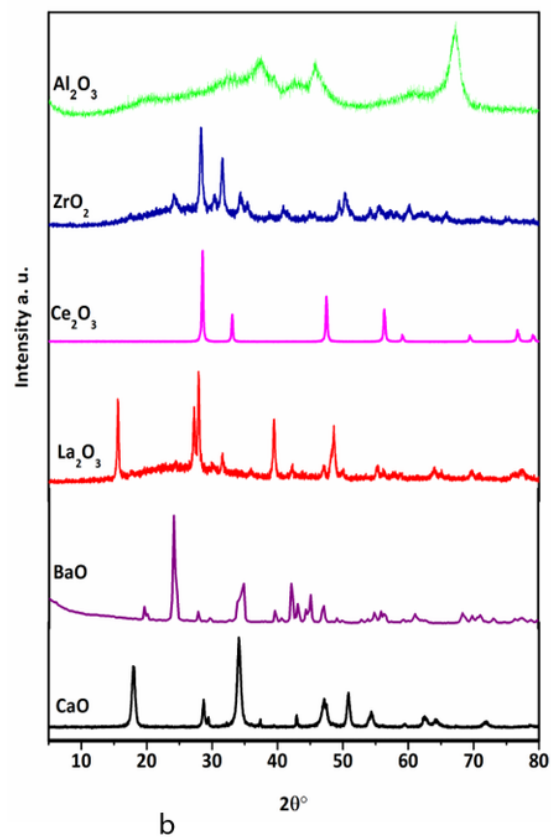
Scheme

Scheme-I is available in the Supplementary Files section.

Figures



a



b

Figure 1

a Chemical structure of NAG, 3A5AF, 3AF and proximicin A.

b PXRD plots for CaO, BaO, La₂O₃, Ce₂O₃, ZrO₂, Al₂O₃ catalyst.

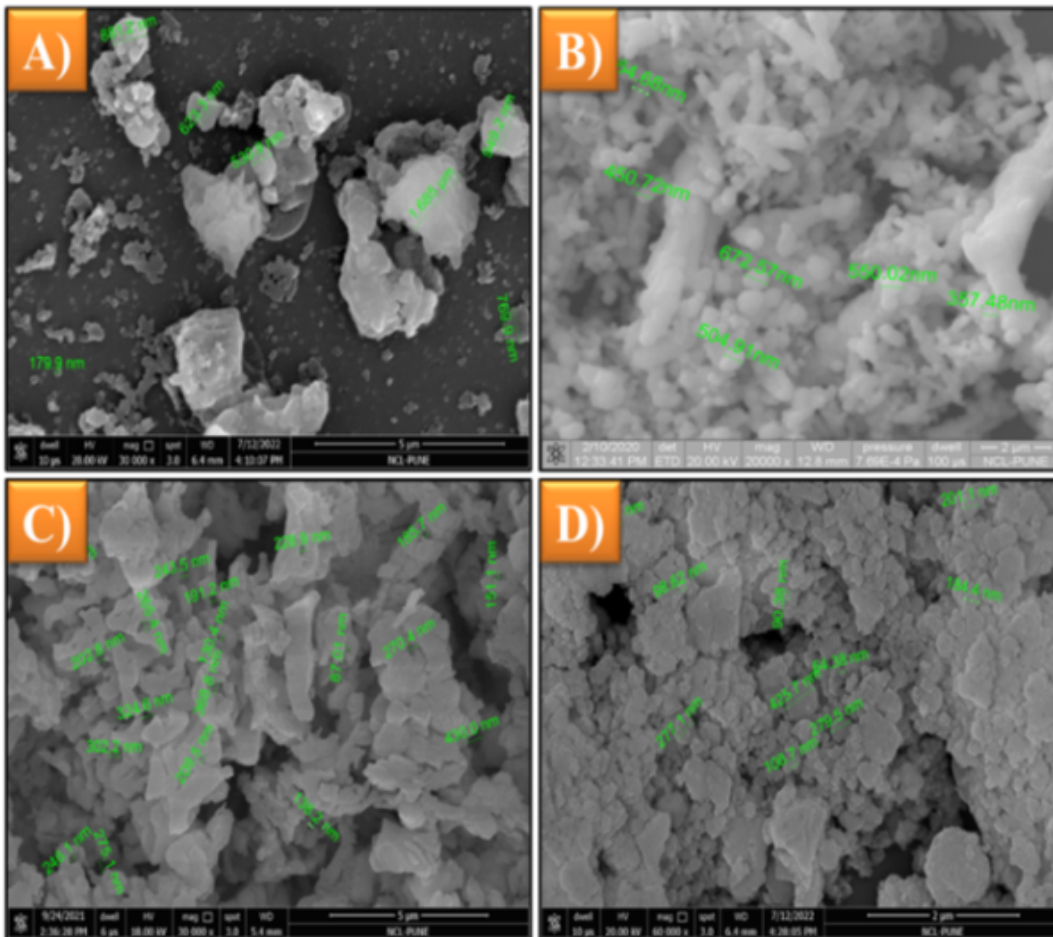


Figure 2

Scanning Electron Micrographs for A) CaO B) BaO C) La₂O₃ and D) Ce₂O₃ catalyst.

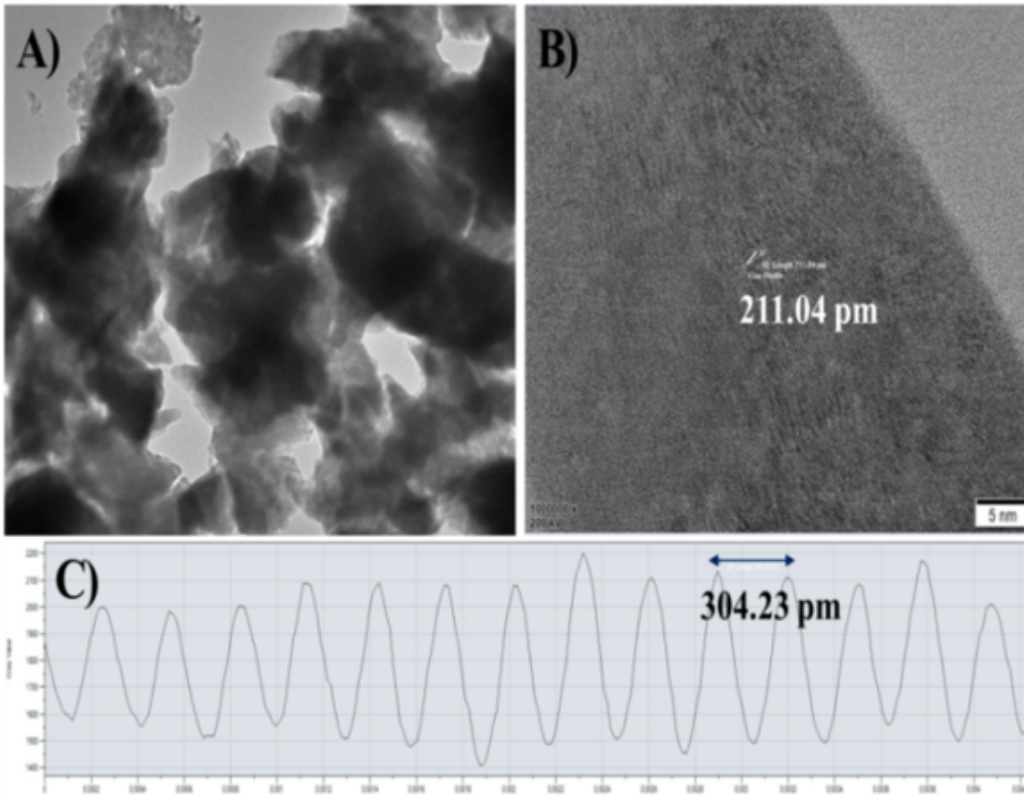


Figure 3

(A-B) Transmission Electron Micrographs La_2O_3 catalyst and (C) d-spacing for La_2O_3 catalyst.

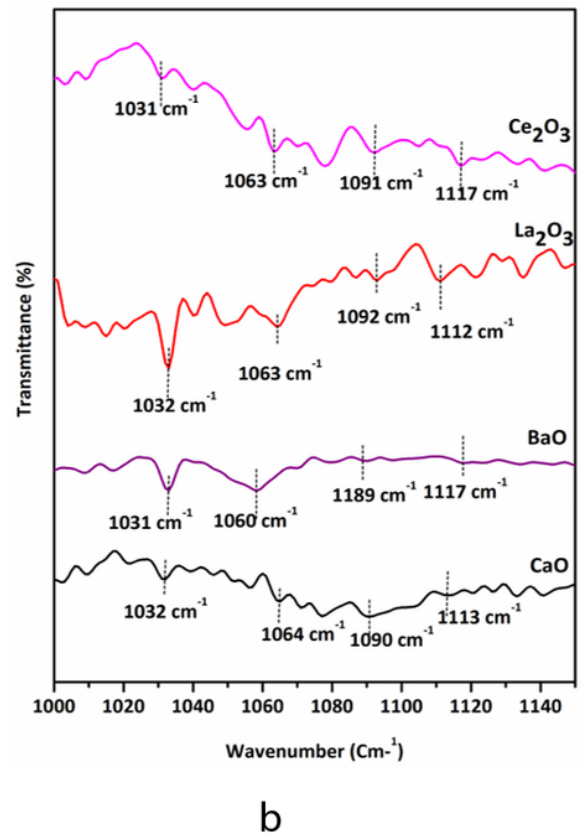
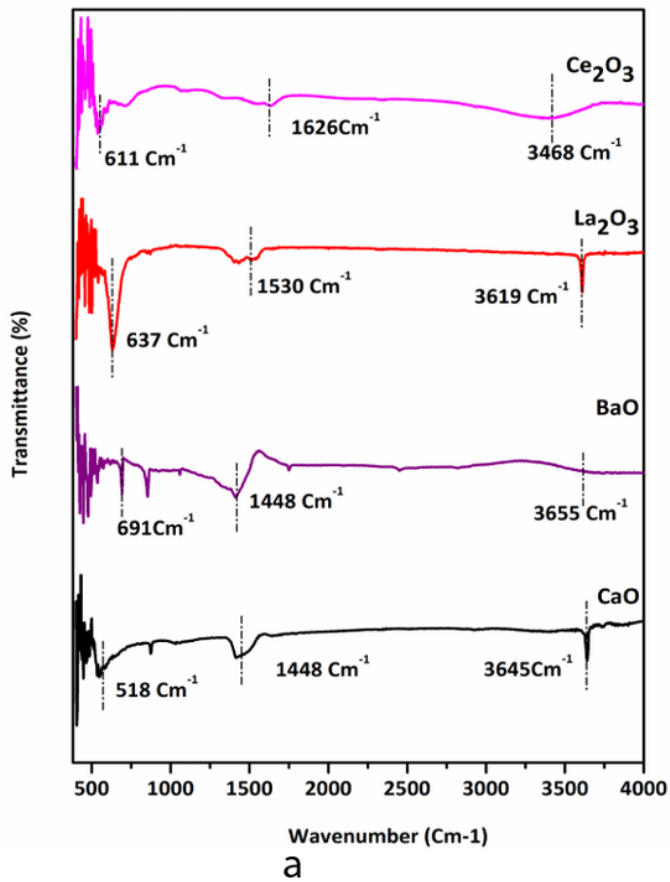


Figure 4

A FT-IR spectra for all metal oxide catalyst

B FT-IR spectra for MeOH adsorbed on all metal oxide catalysts

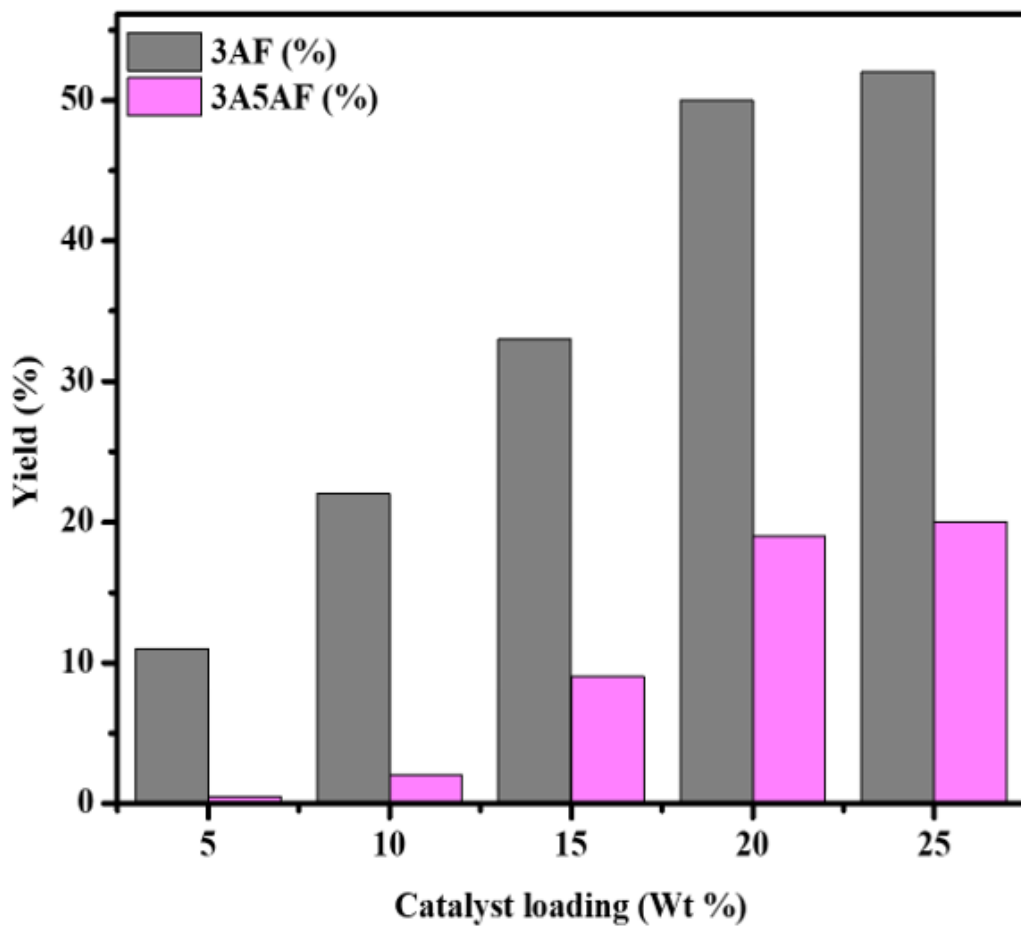


Figure 5

Effect of substrate to catalyst ratios on 3AF production.

Reaction conditions: NAG (1- 5 gm), Dioxane (25 mL), Time (3 h), Temp (180 °C), Catalyst (200 mg).

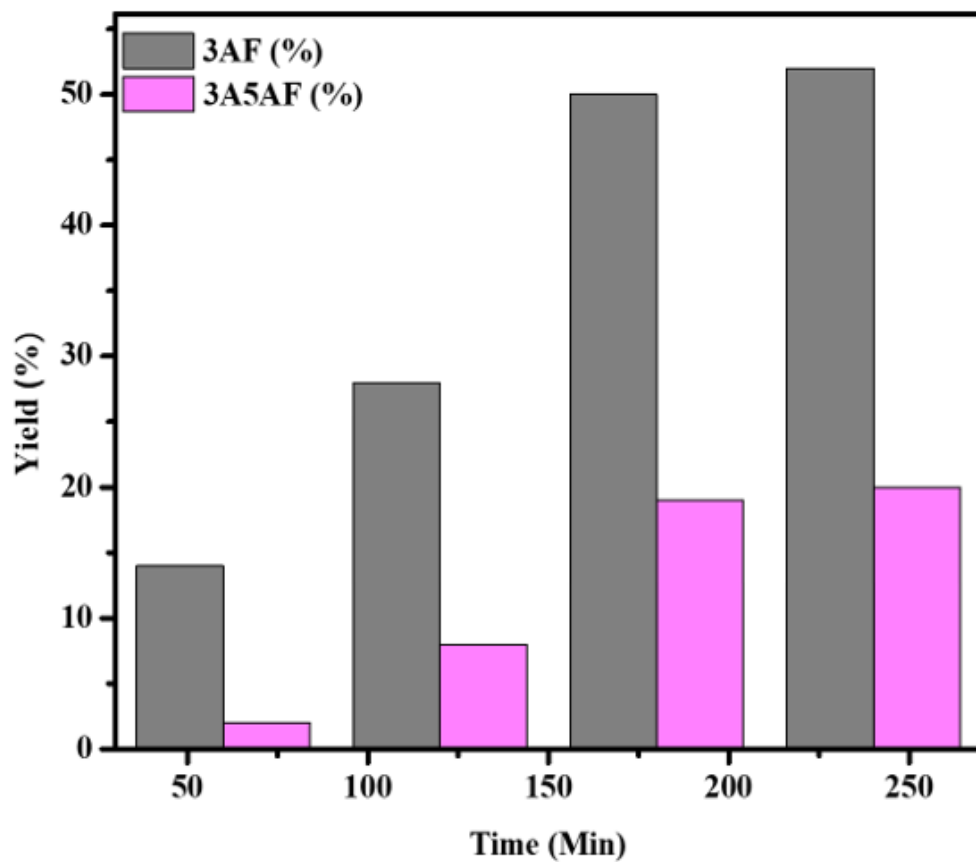


Figure 6

Effect of time on 3AF production.

Reaction conditions: NAG (1 gm), Dioxane (25 mL), Time (3 h), Temp (180 °C), Catalyst (200 mg).

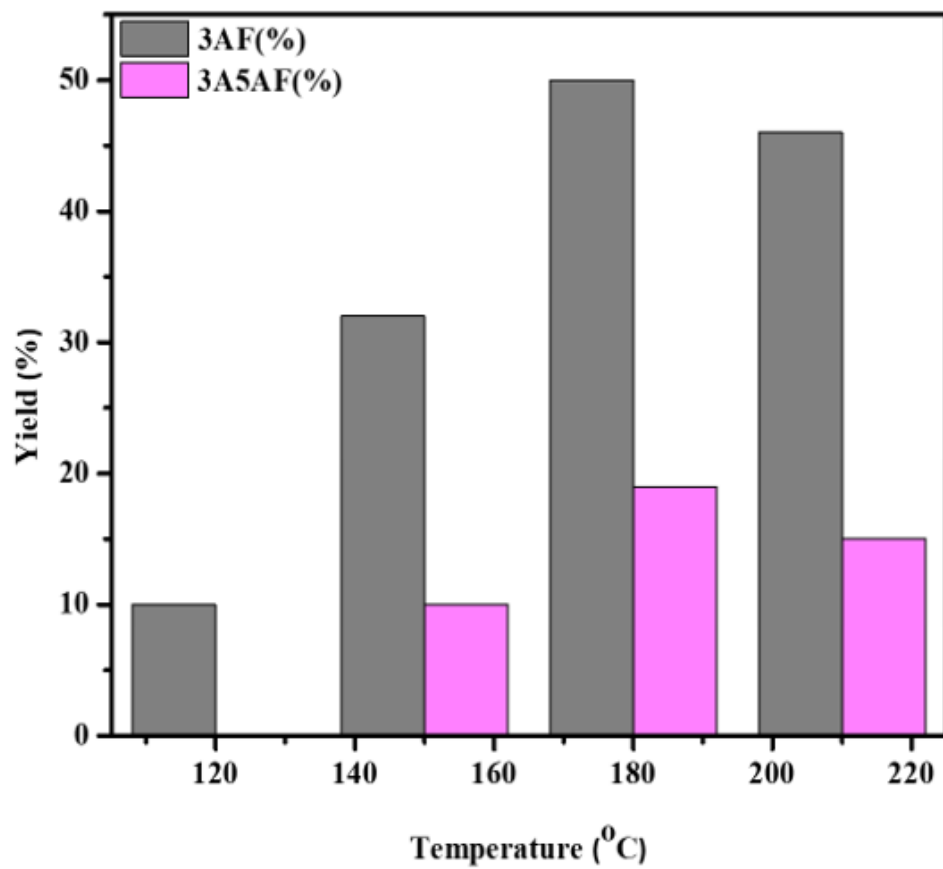


Figure 7

Effect of temperature on 3AF production.

Reaction conditions: Reaction conditions: NAG (1 gm), Dioxane (25 mL), Time (3 h), Temp (180 °C), Catalyst (200 mg).

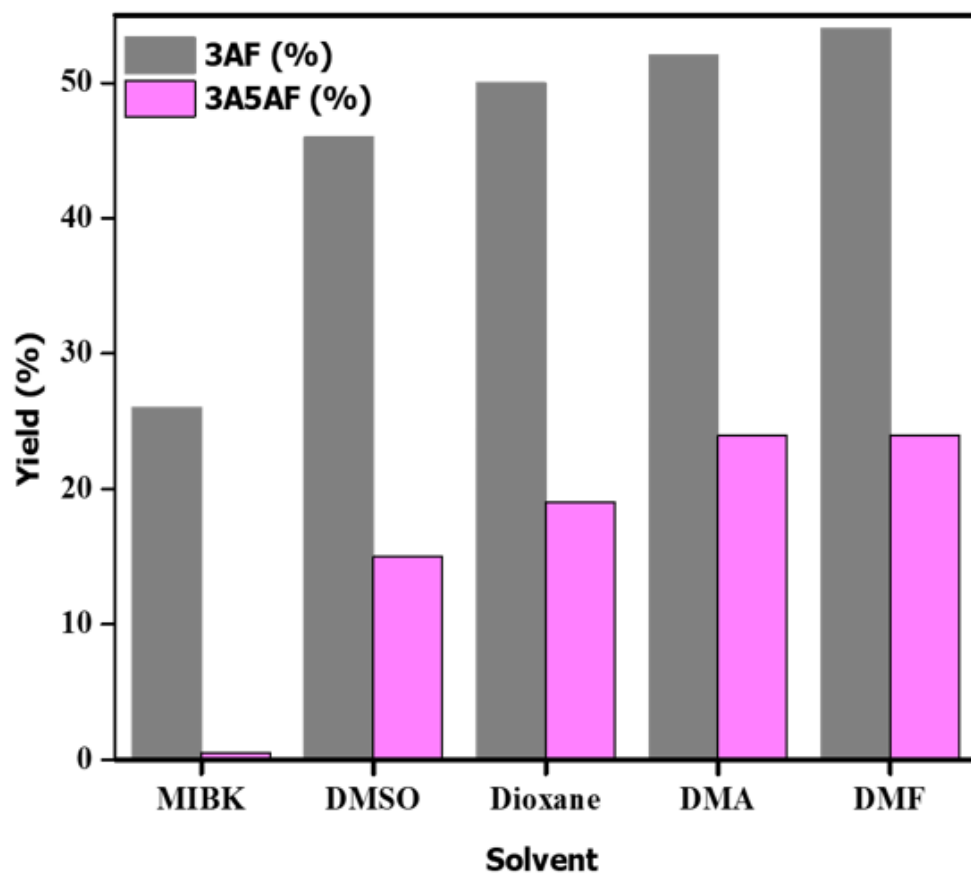


Figure 8

Effect of solvent on 3AF production.

Reaction conditions: NAG (1 gm), Dioxane (25 mL), Time (3 h), Temp (180 °C), Catalyst (200 mg).

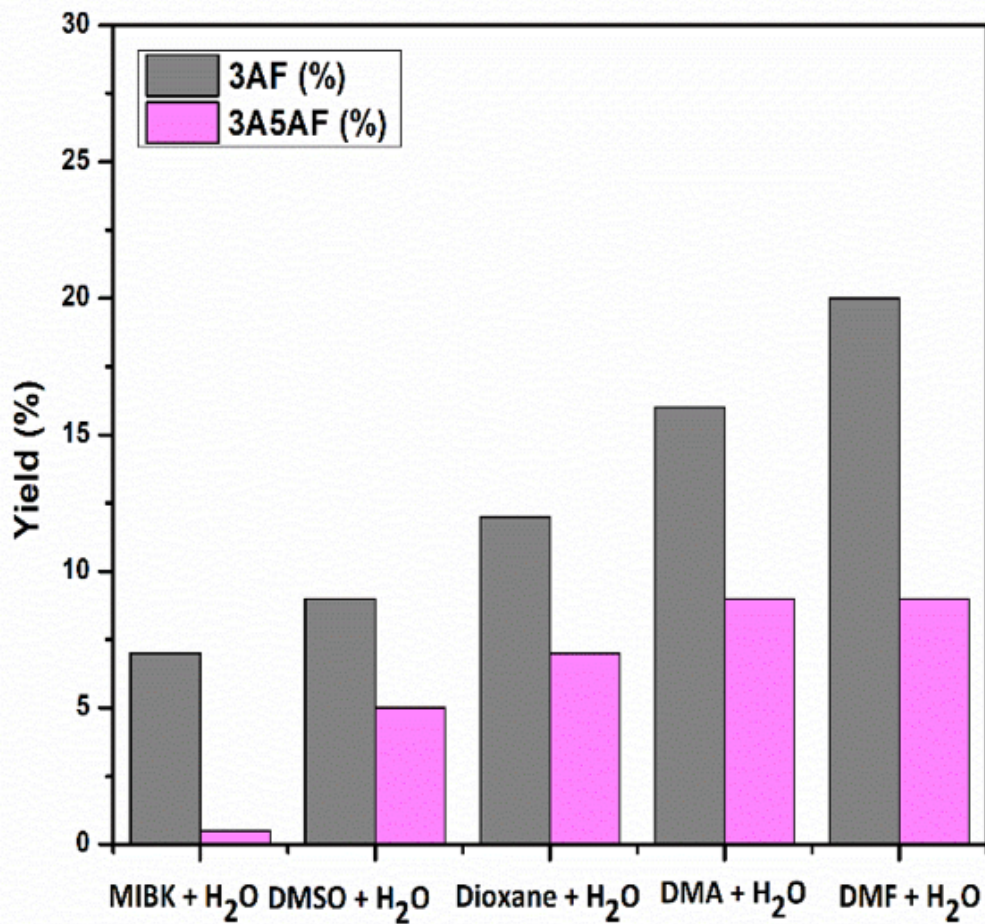


Figure 9

Effect of water on 3AF production.

Reaction conditions: NAG (1 gm), Dioxane (12.5 mL), Water (12.5 mL), Time (3 h), Temp (180 °C), Catalyst (200 mg).

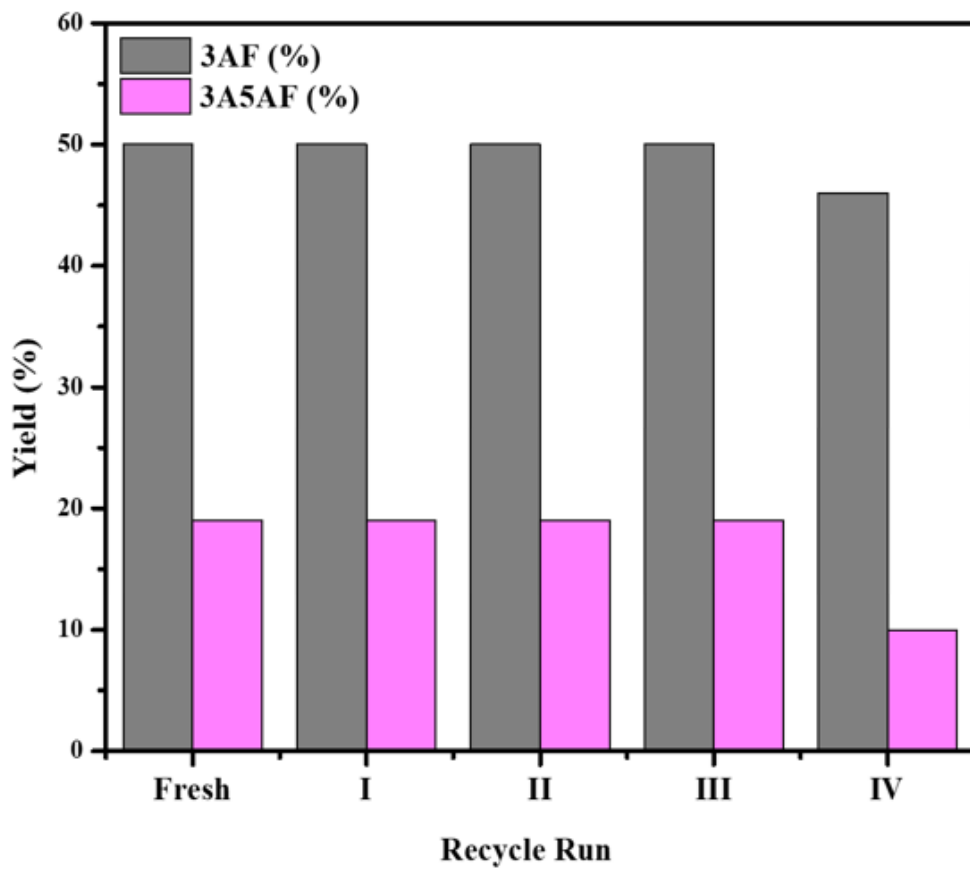


Figure 10

Catalyst recycle study

Reaction conditions: NAG (1 gm), Dioxane (25 mL), Time (3 h), Temp (180 °C), Catalyst (200 mg).

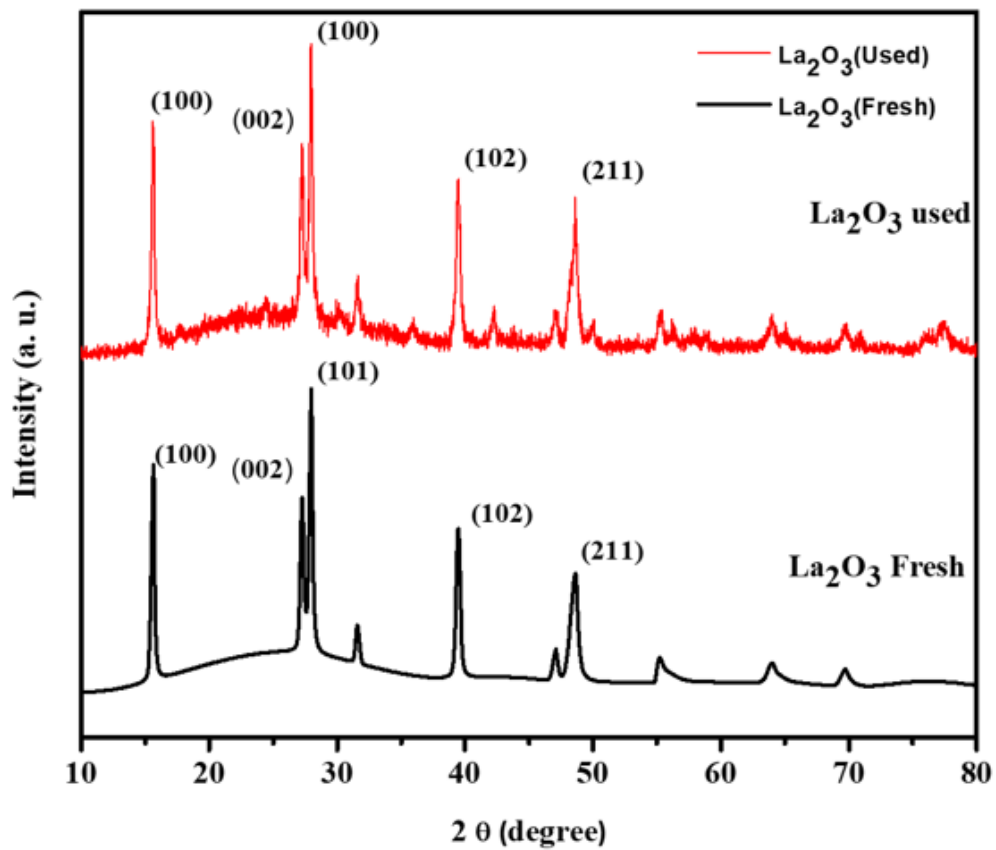


Figure 11

Powder XRD pattern for fresh calcined La₂O₃ and used La₂O₃ metal oxide catalysts

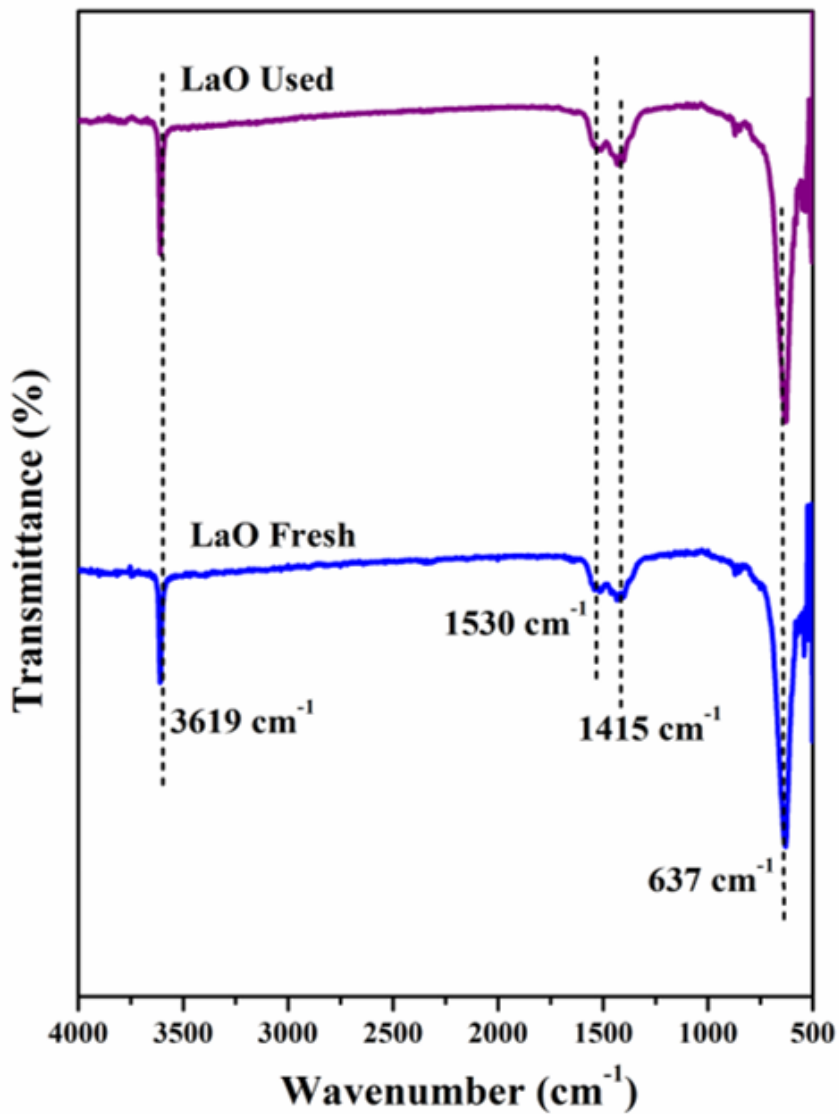


Figure 12

FT-IR spectra for Fresh and used La_2O_3 catalyst

Supplementary Files

This is a list of supplementary files associated with this preprint. Click to download.

- [Scheme1.png](#)
- [SupportinffinalCVRSpringer.docx](#)
- [SYNOPSISITOC.docx](#)